# Hepta-Mode Terminal Microstrip Antenna for Mobile Wi-Fi 6/6E and UWB Channels 5–11 MIMO Applications

Kaifeng Li, Yongjian Zhang, and Yue Li, *Senior Member, IEEE*

***Abstract*— A hepta-mode wideband microstrip antenna is proposed for use on the back cover of mobile terminals, targeting Wi-Fi 6/6E and ultrawideband (UWB) channels 5–11 MIMO applications. This multiple-input multiple-output (MIMO) antenna design comprises four elements arranged in a sequential rotation pattern, each featuring four small patches with two asymmetric notches. Through proper adjustment of patch and notch dimensions, seven modes are effectively excited by a rotated L-shaped feeding probe, thereby amplifying bandwidth of the proposed antenna. In addition, size miniaturization is achieved using a circle of blind vias. To validate the design strategy, a prototype of the MIMO antenna is constructed with dimensions measuring 60.6 × 60.6 × 2 mm$^3$. Meeting the requirements for mobile antenna specifications, the proposed MIMO antenna covers a wide range of frequencies, including Wi-Fi 6/6E and UWB channels 5–11, with a measured −6-dB impedance bandwidth of 5.14–9.05 GHz and an isolation of over 12 dB between each antenna element. Combining broad bandwidth, compact dimensions, and a low profile, this MIMO antenna demonstrates significant potential for supporting diverse wireless services on mobile terminals.**

***Index Terms*— Broadband antennas, microstrip antennas, mobile antennas, multimode antennas, multiple-input multiple-output (MIMO).**

## I. Introduction

With the rapid advancement of mobile communication technologies, such as ultrawideband (UWB) and wireless fidelity (Wi-Fi), there is a growing need for mobile phones to accommodate more antennas to cover an expanding array of frequency bands. In addition, to achieve higher transmission rates, the multiple-input multiple-output (MIMO) technique requires a greater number of antennas [1], [2], [3], [4]. Traditional terminal antennas, typically located in the frame area [5], [6], [7], [8], [9], [10], [11], [12], encounter challenges from spatial constraints. To reconcile the rising demand for antennas with limited space availability, back cover antennas, such as microstrip [13], [14], [15], [16], [17], slot [18], and PIFA [19], [20] antennas, have garnered considerable attention. Microstrip antennas stand out for their low profile and easy integration. However, conventional microstrip antennas are hampered by a narrow bandwidth owing to their high quality factor, which hampers their deployment in terminals.

Currently, three main approaches are commonly utilized to increase the bandwidth of microstrip antennas. The first method incorporates parasitic structures, such as parasitic patches [21], monopoles [22], or distributed circuits [23], [24], to broaden the bandwidth, albeit at the expense of increased space requirements. The second strategy employs frequency-reconfigurable technology [25], [26], [27]. Through specially designed circuits with switching capabilities, antennas can dynamically operate in various narrowband modes, thus achieving broadband performance. The third approach involves coupling multiple modes, often utilizing additional structures, such as slots, notches, and vias, to combine several operational modes for wideband applications [28], [29], [30], [31], [32], [33], [34], [35], [36], [37]. In [28], symmetric notches and two sets of shorting vias are employed to excite $TM_{10}$, $TM_{01}$, and monopole modes, achieving a broad bandwidth of 41%. Similarly, in [30], a broadband antenna with two high-order modes is proposed by adjusting slot and blind via sizes, maintaining a low profile of 0.043 $\lambda_0$ (where $\lambda_0$ is the free-space wavelength at the center frequency). By segmenting patches into periodically arranged rectangular units with gridded [33], [34], [35], [36] or parallel [37] slots, antiphase $TM_{20}$ mode can be excited, resulting in a dual-mode wideband performance with a relative bandwidth of up to 41%. In addition, coupling feeding methods, such as L-shaped probes [38], [39] and slot-coupled lines [40], [41], are commonly employed in multimode designs to facilitate wideband impedance matching. Despite their broadband capabilities, multimode antennas often feature intricate structures and large footprints, limiting their widespread application in terminals. Consequently, designing wideband microstrip antennas with low profiles and compact sizes remains a significant challenge.

In this study, we propose a hepta-mode wideband microstrip antenna positioned on the back cover of mobile terminals for MIMO applications in Wi-Fi 6/6E and UWB channels 5–11. Unlike previous research, we explore additional modes to achieve an even wider bandwidth. Beginning with an antenna element comprising four small patches, we introduce two asymmetric notches on each small patch and utilize a rotated L-shaped feeding probe for impedance matching. This results

Manuscript received 7 May 2024; revised 8 July 2024; accepted 24 July 2024. Date of publication 2 August 2024; date of current version 9 September 2024. This work was supported in part by the National Natural Science Foundation of China under Grant U22B2016, in part by the National Key Research and Development Program of China under Grant 2021YFA0716601, and in part by the China Postdoctoral Science Foundation under Grant GZB20240334 and Grant 2024M751678. *(Corresponding author: Yue Li.)*

The authors are with the Department of Electronic Engineering, Beijing National Research Center for Information Science and Technology, Tsinghua University, Beijing 100084, China (e-mail: lyee@tsinghua.edu.cn).

Color versions of one or more figures in this article are available at https://doi.org/10.1109/TAP.2024.3435031.

Digital Object Identifier 10.1109/TAP.2024.3435031

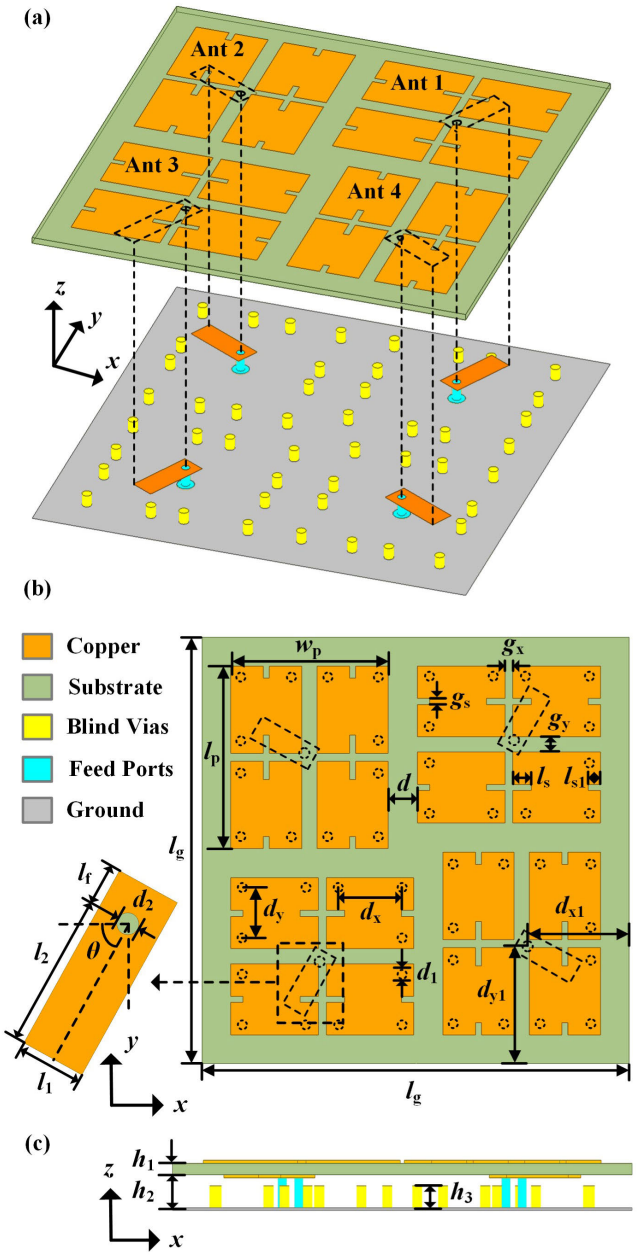


Fig. 1. Geometry configuration of the proposed four-element MIMO antenna. (a) Exploded view. (b) Top view. (c) Side view.

in the simultaneous excitation of seven modes and a broad bandwidth across the four patches. In addition, employing a circle of blind vias enables size reduction of the antenna element, allowing the MIMO antenna to accommodate the limited space typical of mobile phones. We fabricated and measured a prototype of the proposed MIMO antenna, confirming its coverage of a wide bandwidth of 5.14–9.05 GHz within a compact dimension of 60.6 × 60.6 × 2 mm$^3$. These results underscore the significant potential of the proposed MIMO antenna for mobile Wi-Fi and UWB applications.

## II. Antenna Configuration and Operating Modes

The proposed MIMO antenna's geometric configuration is depicted in Fig. 1, while Table I lists the optimized dimensions. Comprising four identical antenna elements

TABLE I

Dimensions of the Proposed Design With $\theta = 61°$ (Unit: mm)

| $l_g$ | $l_p$ | $w_p$ | $d$ | $g_x$ | $g_y$ | $l_s$ |
|---|---|---|---|---|---|---|
| 70 | 30 | 25.8 | 4.8 | 1.3 | 2.5 | 3 |
| $l_{s1}$ | $g_s$ | $d_x$ | $d_y$ | $d_1$ | $d_{x1}$ | $d_{y1}$ |
| 2 | 1 | 10.35 | 8.21 | 1.5 | 16.73 | 19.22 |
| $l_1$ | $l_2$ | $l_f$ | $d_2$ | $h_1$ | $h_2$ | $h_3$ |
| 3.9 | 9.1 | 1.65 | 1.3 | 0.5 | 1.5 | 1.35 |

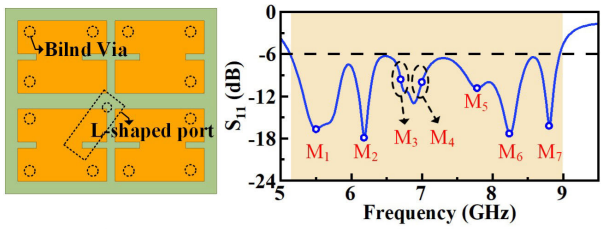


| $M_i$ | $M_1$ | $M_2$ | $M_3$ | $M_4$ | $M_5$ | $M_6$ | $M_7$ |
|---|---|---|---|---|---|---|---|
| Mode Name | $TM_{10}$ + $TM_{\bar{2}0}$ | $TM_{01}$ + $TM_{0\bar{2}}$ | $TM_{2\bar{0}}$ | $TM_{\bar{0}2}$ | monopole mode | $TM_{\bar{2}2}$ | $TM_{22}$ |

(c)

Fig. 2. (a) Top view of the antenna element. (b) Simulated reflection coefficient of the antenna element. $M_i$ represents the $i$th resonant mode in the band. (c) Names of the seven resonant modes above.

labeled as Ants 1–4 in Fig. 1(a), arranged in a sequential rotation pattern, the antenna structure is supported by a dual-layer configuration with a footprint of $l_g \times l_g$. The upper layer, an FR4 substrate ($\varepsilon_r = 4.4$ and $\tan\delta = 0.02$), has a thickness of $h_1$, while the lower layer is an air layer with a thickness of $h_2$, as illustrated in Fig. 1(c). Each antenna element is rectangular, sized $l_p \times w_p$, and positioned at a distance of $d$ from adjacent elements. One antenna element comprises four small patches on the substrate's top layer, an L-shaped probe with a narrow strip on the bottom layer, and 12 equally tall metal columns connected to the bottom metal ground. The small patches are spaced $g_x$ apart in the $x$-axis direction and $g_y$ in the $y$-axis direction, with two asymmetric notches, sized $g_s \times l_s$ and $g_s \times l_{s1}$, etched on their edges. The detailed structure of the top narrow strip of the L-shaped probe is depicted in the inset of Fig. 1(b), featuring dimensions $l_1 \times (l_2 + l_f)$ and a rotation angle $\theta$ relative to the long side of the antenna element. Positioned symmetrically around each antenna element between the substrate and the metal ground, 12 metal columns with a height of $h_3$ and a diameter of $d_1$ are located. Serving as both the dielectric back cover and the space between the mainboard and the back cover, this dual-layer configuration aligns with typical mobile phone designs.

To elucidate the operational principle of the suggested MIMO antenna, we first examine an individual antenna element. Fig. 2(a) depicts the top view of the antenna element, featuring four small patches with two asymmetric notches, a rotated L-shaped feeding probe, and a circle of blind vias. Through meticulous adjustment of the size and placement of these elements, seven resonant modes are concurrently excited,

facilitating a wide bandwidth of 5.13–9 GHz, as evidenced by the simulated reflection coefficient depicted in Fig. 2(b). Furthermore, the specific dimensions of the individual antenna element deviate slightly from those of the entire MIMO antenna, with $l_2$ measuring 9 mm and $l_f$ measuring 1.9 mm. Fig. 2(c) labels the seven operating modes for the proposed antenna element. In a microstrip antenna oriented in the $xoy$ plane and orthogonal to the $z$-axis, resonant modes $TM_{mn}$ are typically induced. Here, $m$ and $n$ denote the electric-field's distribution over $m$ half-wavelengths along the $x$-axis and $n$ half-wavelengths along the $y$-axis. Moreover, if $m$ or $n$ is denoted as $\overline{m}$ or $\overline{n}$, it signifies a phase reversal of the electric field at the midpoint of the patch side along the $x$-axis or $y$-axis. For convenience, these seven modes are denoted as $M_i$, representing the $i$th resonant mode of the proposed antenna element within the operating frequency band.

In this study, owing to the multimode coupling method and asymmetric feeding structure, the modes of the proposed antenna element exhibit a degree of impurity. To provide a more fundamental understanding of the operating modes, we have identified seven resonant frequencies with relatively pure modes based on electric-field distributions and radiation patterns, as depicted in Fig. 3. These seven modes can be categorized into three mode pairs and one monopole mode, as observed from the electric-field distributions. Each mode pair comprises $TM_{mn}$ and $TM_{nm}$ modes, exhibiting approximately symmetrical 90° rotation of electric-field distributions and 3-D radiation patterns about the $z$-axis. Because the proposed antenna element has a rectangular shape, $TM_{mn}$ and $TM_{nm}$ modes are nondegenerate. For clarity, we will detail one mode from each mode pair below. The first mode pair includes $TM_{10} + TM_{\overline{2}0}$ ($M_1$) and $TM_{01} + TM_{0\overline{2}}$ ($M_2$). Mode $TM_{10} + TM_{\overline{2}0}$ represents a hybrid mode featuring an antiphase double-half-wavelength electric-field distribution along the $x$-axis and a uniform distribution along the $y$-axis. Consequently, equivalent magnetic currents are generated in the same direction on the radiation apertures, resulting in a broadside radiation pattern. The second mode pair comprises $TM_{2\overline{0}}$ ($M_3$) and $TM_{\overline{0}2}$ ($M_4$). Mode $TM_{2\overline{0}}$ exhibits an antiphase uniform amplitude distribution along the $y$-axis and a double-half-wavelength distribution along the $x$-axis. The directions of equivalent magnetic currents are opposite on the radiation apertures, leading to a conical radiation pattern. A slight coupling exists between modes $M_3$ and $M_4$ owing to their close resonant frequencies, causing some deviations between actual and theoretical field distributions. The third mode pair includes $TM_{\overline{2}\overline{2}}$ ($M_6$) and $TM_{2\overline{2}}$ ($M_7$). The electric field of $TM_{\overline{2}\overline{2}}$ displays a double-half-wavelength distribution along both the $x$-axis and $y$-axis, with an extra phase reversal along the $x$-axis. Similar to the $TM_{2\overline{0}}$ mode, the radiation pattern of $TM_{\overline{2}\overline{2}}$ is conical. The monopole mode ($M_5$) exhibits an electric field symmetrically distributed along the diagonal of the antenna element, generating an equivalent magnetic current for the conical radiation pattern.

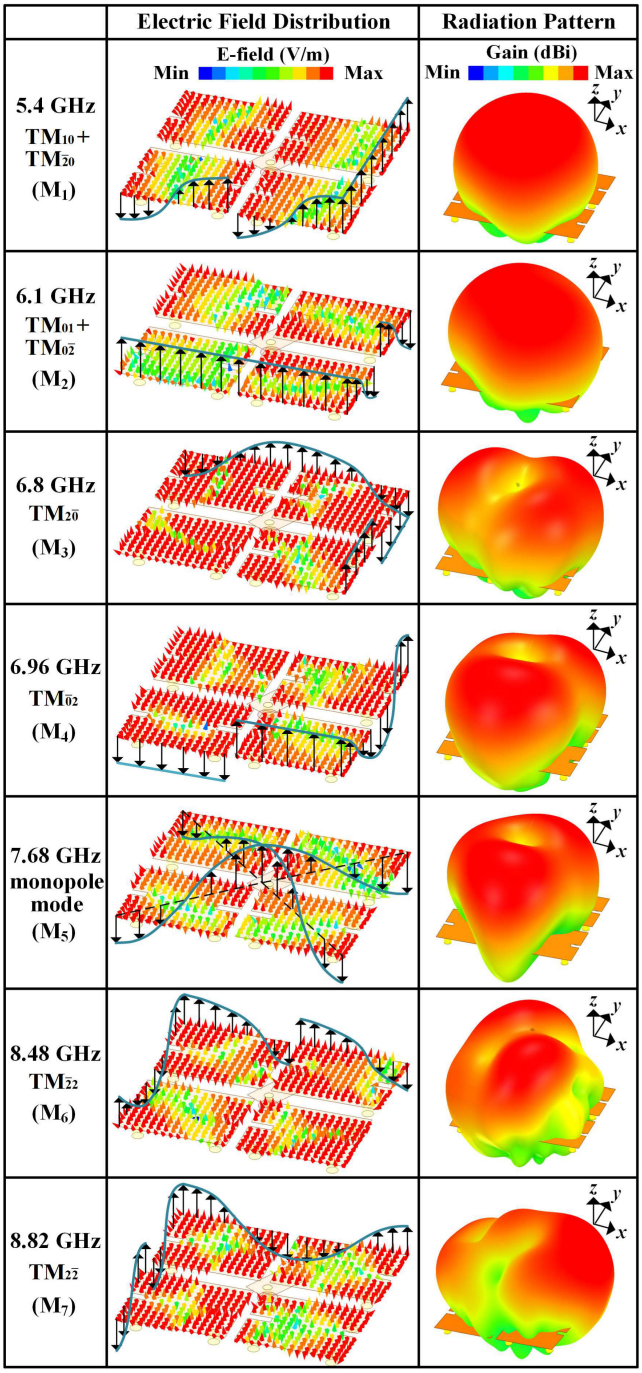


Fig. 3. Electric-field distributions and 3-D radiation patterns of the proposed antenna element at seven resonant frequencies.

## III. Antenna Evolution and Parametric Analysis

Microstrip antennas can be analyzed using the equivalent circuit theory of transmission lines. As demonstrated in [42], transmission lines' effective permeability or permittivity correlates positively with the series or shunt capacitance of the equivalent circuit. Moreover, based on the relationship between resonant frequency and electrical length, it can be inferred that the resonant frequency inversely correlates with the effective permeability and permittivity. Thus, tuning the component values of the equivalent circuit of the microstrip antenna enables adjustment of the resonant frequency.

Using the abovementioned approach, the microstrip antenna proposed achieves multimode broadband performance through specialized structural design, as depicted in Fig. 4. Initially, Ant A is divided into four small patches with two

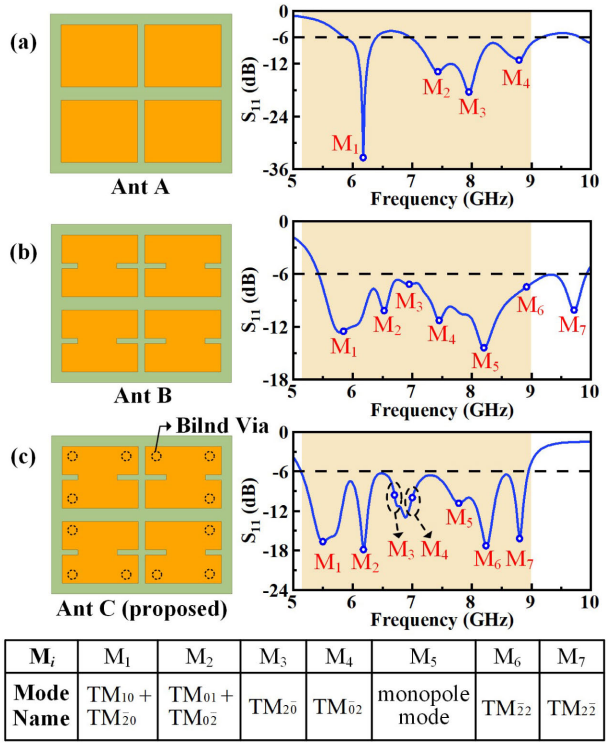


| $\mathbf{M}_i$ | $M_1$ | $M_2$ | $M_3$ | $M_4$ | $M_5$ | $M_6$ | $M_7$ |
|---|---|---|---|---|---|---|---|
| **Mode Name** | $TM_{10}+TM_{\bar{2}0}$ | $TM_{01}+TM_{0\bar{2}}$ | $TM_{2\bar{0}}$ | $TM_{\bar{0}2}$ | monopole mode | $TM_{\bar{2}2}$ | $TM_{2\bar{2}}$ |

Fig. 4. Evolution process of the proposed antenna element and the corresponding reflection coefficients. (a) Ant 1: four small patches. (b) Ant 2: add notches on the short side. (c) Ant 3: add a circle of blind vias.

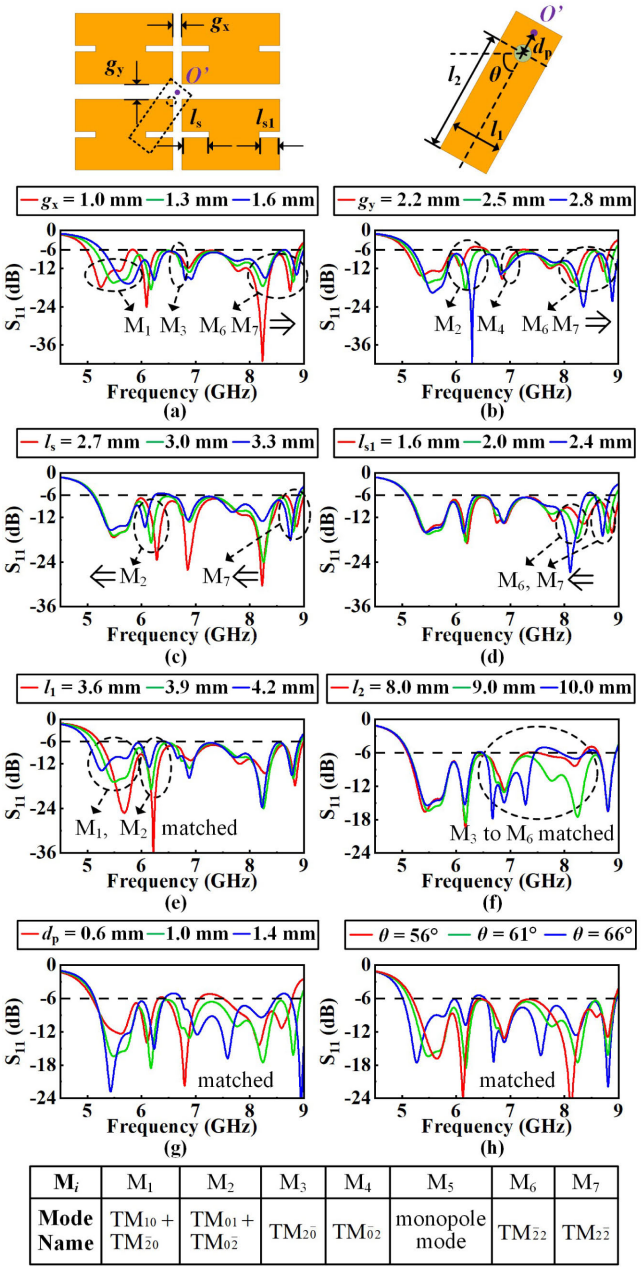


| $\mathbf{M}_i$ | $M_1$ | $M_2$ | $M_3$ | $M_4$ | $M_5$ | $M_6$ | $M_7$ |
|---|---|---|---|---|---|---|---|
| **Mode Name** | $TM_{10}+TM_{\bar{2}0}$ | $TM_{01}+TM_{0\bar{2}}$ | $TM_{2\bar{0}}$ | $TM_{\bar{0}2}$ | monopole mode | $TM_{\bar{2}2}$ | $TM_{2\bar{2}}$ |

Fig. 5. Reflection coefficients for different parameters of the proposed antenna element. (a) $g_x$. (b) $g_y$. (c) $l_s$. (d) $l_{s1}$. (e) $l_1$. (f) $l_2$. (g) $d_p$. (h) $\theta$.

perpendicular slots, effectively adding two series capacitors in the equivalent circuit of Ant A. By adjusting the width of these slots, the value of the series capacitors is tuned, thereby bringing the four lower modes $M_1$–$M_4$ closer together. Eight symmetrical notches are etched on Ant A to further broaden the bandwidth to create Ant B. These notches extend the surface current path of the patches, effectively increasing the electrical lengths of the modes and reducing their resonant frequencies. Consequently, the frequencies of the higher modes $M_5$–$M_7$ decrease significantly, facilitating the simultaneous excitation of seven modes for wideband performance, as depicted in Fig. 4(b). However, the achieved broadband results do not encompass the target frequency band. Ant C with a circle of blind vias is introduced to address this without increasing the antenna size or compromising broadband performance. These blind vias act as parallel-plate capacitors between the patches and the ground. By adjusting the diameter or height of these blind vias, the shunt capacitance of the equivalent circuit for Ant C increases, consequently increasing the effective permittivity and lowering the overall bandwidth of the antenna. As depicted in Fig. 4(c), the proposed antenna element covers the target band from 5.13 to 9 GHz through the excitation of seven modes.

To further illustrate the control of the seven modes, an analysis of certain critical parameters is shown in Fig. 5. First, the widths of the two perpendicular slots are examined with the simulated reflection coefficients in Fig. 5(a) and (b). The slot parallel to the short side disrupts the surface current along the $x$-axis, effectively introducing a series capacitor. Therefore, as the slot width $g_x$ increases, the series capacitance decreases, increasing the resonant frequencies of modes $M_1$, $M_3$, $M_6$, and $M_7$, whose surface currents have components along the $x$-axis. Similarly, as the width $g_y$ increases, the resonant frequencies of modes $M_2$, $M_4$, $M_6$, and $M_7$ rise owing to the interrupted current components along the $y$-axis. Second, the lengths of the notches are analyzed in Fig. 5(c) and (d). The notches on the short side are positioned at the midpoint of the small patches, where the current peaks of $TM_{\bar{2}2}$ and $TM_{2\bar{2}}$ modes are located. When $l_{s1}$ is lengthened, the electrical lengths of $M_6$ and $M_7$ stretch, causing a downward shift in their resonant frequencies. Moreover, $M_2$ is a hybrid mode coupled through the slot. Thus, as the

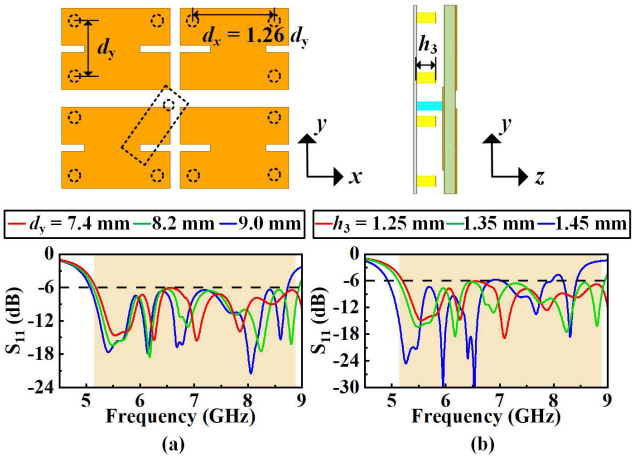


Fig. 6. Analyses of different parameters of the blind vias. (a) $d_y$. (b) $h_3$.

lengths $l_s$ of the notches on the slot increase, the resonant frequencies of $M_2$ and $M_7$ decrease. Third, the main parameters affecting impedance matching are studied. The size of the L-shaped probe's narrow strip significantly influences the feeding port's capacitance and inductance. As shown in Fig. 5(e), the strip width $l_1$ mainly impacts the impedance matching of low-frequency modes by changing the series capacitance of the port, thus affecting the frequencies of modes $M_1$ and $M_2$. Similarly, Fig. 5(f) shows that the length of strip $l_2$ primarily affects the impedance matching of the high-frequency modes $M_3$–$M_6$ by adjusting the series inductance of the port. In addition, owing to the varying input impedance of the antenna at different positions, the port location also determines the matching of all seven modes. As illustrated in Fig. 5(g) and (h), changes in the distance $d_p$ from the metallic column to the center $O'$ of the antenna element or the rotation angle $\theta$ of the narrow strip significantly affect the matching of each mode. Furthermore, the diameter $d_2$ of the metallic column slightly impacts antenna performance. Ultimately, by appropriately adjusting these parameters, the seven modes can be tuned through the asymmetric slots or notches and excited simultaneously by the L-shaped probe, thereby achieving broadband performance.

To further illustrate the principle of size miniaturization, we analyzed the position and size of the blind vias. As depicted in Fig. 6(a), the distance ratio between adjacent blind vias along the $x$-axis and $y$-axis is fixed at 1.26, which matches the aspect ratio of the small patch. As the distance $d_y$ increases, the blind vias move closer to the edge of the small patch, where the electric field is stronger. This results in a larger equivalent capacitance of the blind vias, causing the frequency decrease across the whole band. Similarly, as shown in Fig. 6(b), increasing the height $h_3$ of the blind vias reduces the distance between the blind vias and the small patches, which increases the equivalent capacitance and causes a downward shift in the frequencies of all seven modes. By appropriately adjusting the position and size of the blind vias, it is possible to achieve size miniaturization by lowering the frequency band without increasing the antenna's physical dimensions.

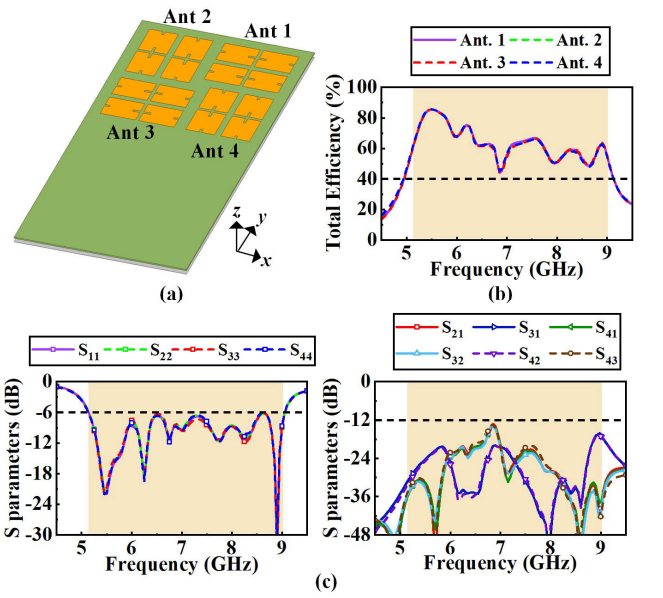


Fig. 7. Analysis of the proposed antenna integrated on a common ground layer. (a) Configuration. (b) Total efficiencies. (c) S-parameters.

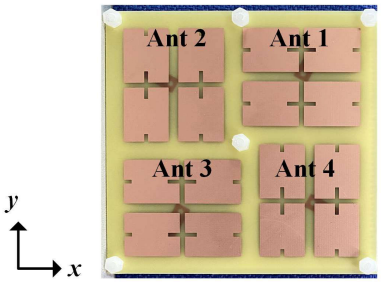


Fig. 8. Top view of the fabricated four-element MIMO antenna prototype.

Based on the proposed antenna element, we developed a four-element MIMO array. We arranged these four elements in a sequential rotation style and optimized their spacing to achieve high isolation within a compact size. To demonstrate the practical applicability of the proposed MIMO antenna, we integrated it with a common mobile phone's ground layer. As shown in Fig. 7(a), both the substrate and ground layers measure 156 × 70 $mm^2$, typical of a smartphone. The MIMO antenna is placed on the upper half of the back cover, maintaining the dimensions listed in Table I. Fig. 7(b) and (c) present simulated total efficiencies and S-parameters of the proposed MIMO antenna. The S-parameters closely match those of the initial design, with the −6-dB impedance band covering Wi-Fi 6/6E and UWB channels 5–11 and isolations exceeding 12 dB. The total efficiencies of all four antenna elements remain above 40% across the operating frequency band, which is sufficiently high for terminal antennas. Overall, these additional simulation results confirm the feasibility and practicality of the proposed antenna design.

## IV. Fabrication and Measurement

A prototype of the proposed MIMO antenna was fabricated and measured to validate the design strategy. Fig. 8 shows

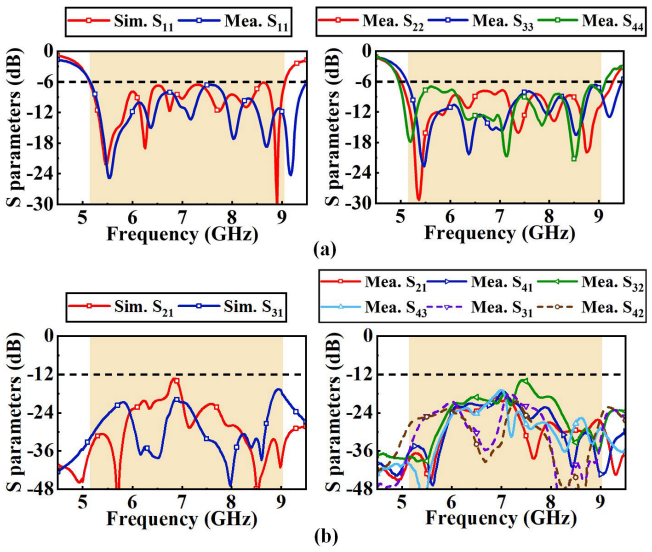


Fig. 9. Simulated and measured S-parameters of the proposed four-element MIMO antenna. (a) Reflection coefficients. (b) Transmission coefficients.

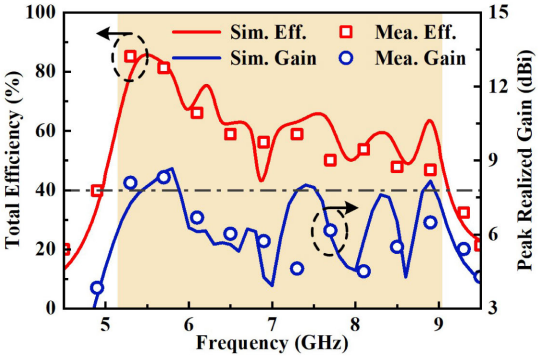


Fig. 10. Total efficiencies and peak realized gains of the proposed MIMO antenna in simulated and measured results.

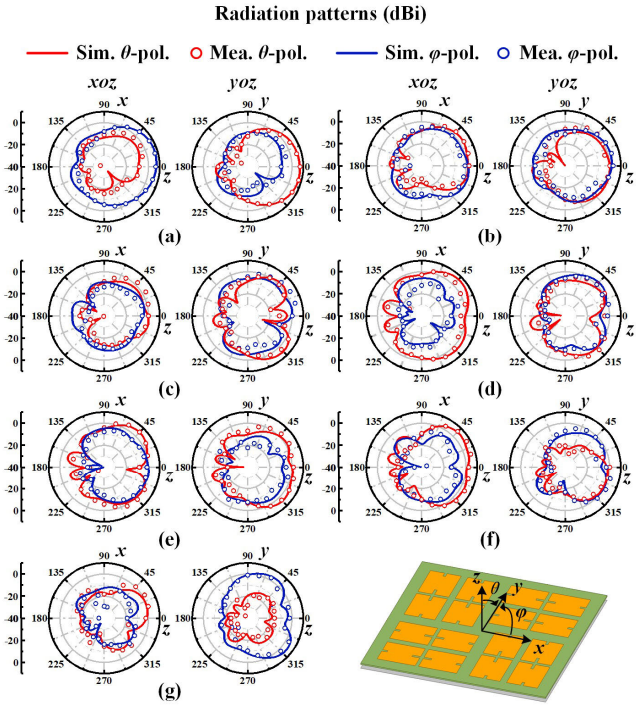


Fig. 11. Simulated and measured 2-D radiation patterns of the proposed four-element MIMO antenna at (a) 5.5, (b) 6.1, (c) 6.7, (d) 7.1, (e) 7.7, (f) 8.5, and (g) 8.9 GHz.

a photograph of the fabricated antenna. The patches of the entire antenna are printed on an FR-4 substrate board using the printed circuit board (PCB) process. Utilizing computer numerical control (CNC) technology, the copper ground plane and blind vias are integrated and processed. Six cylindrical columns with a 1-mm radius and a relative permittivity of 3.0 support the FR-4 substrate board above the copper ground board. In addition, the ground plane has four holes soldered to the outer conductors of four subminiature A (SMA) cable connectors. The inner conductors, serving as the metallic columns of the L-shaped probes, are soldered to the four strips of the L-shaped probes on the lower surface of the substrate. The proposed four-element MIMO antenna was numerically simulated and optimized using the commercial electromagnetic simulation software HFSS 2023 R1. The fabricated prototype was tested with an N9917A vector network analyzer and a standard microwave anechoic chamber.

The simulated and measured S-parameters of the proposed four-element MIMO antenna are shown in Fig. 9. The measured reflection coefficients of all four antenna elements exhibit a broad −6-dB impedance bandwidth ranging from 5.14 to 9.05 GHz, effectively covering the Wi-Fi 6/6E and UWB channels 5–11 bands. As shown in Fig. 9(a), the measured reflection coefficients closely align with the simulated modes. It is also worth noting that the effective permittivity of the FR-4 substrate tends to decrease at frequencies above 7.0 GHz, leading to a noticeable upward shift in the resonant frequencies. As illustrated in Fig. 9(b), the simulated and measured isolations between any two elements exceed 12 dB.

The total efficiency and peak realized gain are measured and shown in Fig. 10. Within the desired band, the simulated peak realized gain ranges from 3.9 to 8.6 dBi, and the total efficiency is above 43.2%. Owing to structural symmetry, only the total efficiency of Ant 1 is presented, ranging from 43.6% to 85.1%. Similarly, the measured peak realized gain of Ant 1 is shown, varying from 4.5 to 8.3 dBi within the band, consistent with the simulated results. Fig. 11 illustrates the 2-D radiation patterns of Ant 1 in the *xoz* and *yoz* planes at the resonant frequencies of all seven modes. The measured results closely match the simulated ones in both $\theta$- and $\varphi$-polarizations, demonstrating broadside or conical radiation characteristics. Although the proposed antenna's radiation patterns and realized gain are somewhat unstable, they remain acceptable for MIMO applications in mobile terminals. Furthermore, based on the simulated and measured far-field radiation patterns, the envelope correlation coefficients (ECCs) between the antenna elements are calculated and provided in Fig. 12. Both $\rho_{12}$ and $\rho_{13}$ are less than 0.04 across the entire band, which is considerably low for

TABLE II
COMPARISON AMONG THE PROPOSED ANTENNA AND OTHER BACK COVER ANTENNAS

| Ref. | Antenna Type | Layer | Feeding Type | Element Dimensions ($\lambda_L^3$) | Number of Modes | -6 dB Bandwidth | Isolation (dB) | Efficiency | Gain (dBi) |
|---|---|---|---|---|---|---|---|---|---|
| [14] | Microstrip antenna | 1 | Coaxial line | 0.24 × 0.24 × 0.047 | 1 | 4.7-5.0 GHz (6.2%) | > 25 | 63%-90%* | N. A. |
| [15] | Microstrip antenna | 1 | Microstrip line | 0.52 × 0.52 × 0.018 | 2 | 4.37-5.5 GHz (22.9%) | > 22 | 40%-50% | 1.9-3.7 |
| [16] | Microstrip antenna | 1 | Coaxial line | 0.59 × 0.30 × 0.012 | 3 | 4.4-5.04 GHz (13.6%) | > 18 | 42%–86% | 3.1-7.2 |
| [17] | Microstrip antenna | 3 | Coaxial line | 0.25 × 0.25 × 0.034 | 2 | 5.13-5.86 GHz (13.3%) | > 12 | 45%-65% | 0.6-3.3 |
| [18] | Slot antenna | 2 | GCPW** | 0.23 × 0.23 × 0.011 | 1 | 3.3-4.2 GHz (24.0%) | > 9.5 | 40%-58% | N. A. |
| [19] | PIFA | 3 | L-shaped line | $\pi \times 0.085^2 \times 0.022$ | 2 | 3.3-4.2 GHz (24.0%) | > 9.7 | 36%-40% | N. A. |
| **Pro.** | **Microstrip antenna** | **2** | **L-shaped probe** | **0.51 × 0.44 × 0.034** | **7** | **5.14-9.05 GHz (55.1%)** | **> 12** | **44%-85%** | **4.5-8.3** |

*: estimated value according to the figure in the paper.
**: grounded coplanar waveguide.
$\lambda_L$: free-space wavelength at the lowest frequency in the band.

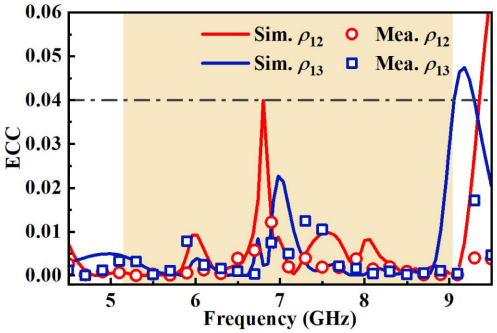


Fig. 12. Simulated and measured ECCs of the proposed four-element MIMO antenna.

mobile MIMO antennas. The measured results indicate that the proposed MIMO antenna is well suited for mobile Wi-Fi and UWB applications.

To highlight the performance advantages of the proposed antenna, Table II compares its performance with other back cover antennas reported in the literature. Various types of antennas, such as microstrip antennas [14], [15], [16], [17], conjoined open-slot antennas [18], and planar inverted-F antennas (PIFAs) [19], are employed for diverse mobile MIMO applications. In a similar footprint area, antennas in [15] and [16] achieve narrower bandwidths with only two or three resonant modes. Despite a smaller footprint, the narrowband antennas in [14] and [17] exhibit a lower bandwidth-to-volume ratio. The broadband antennas in [18] and [19] show lower isolation and efficiency, limiting their utility in mobile MIMO antenna applications. Moreover, compared with some ultra-wideband antennas with smaller dimensions and simpler structures, such as monopole [43], [44] and slot [45], [46] antennas, our antenna uniquely integrates into the mainboard of mobile terminals. In short, the comparison shows that our design offers broader bandwidth with seven modes while maintaining physical dimensions comparable to those of previous back cover antennas. The proposed MIMO antenna demonstrates valuable applications across multiple mobile communication bands.

## V. CONCLUSION

In this study, we propose a hepta-mode wideband microstrip antenna positioned on the terminal's back cover for mobile Wi-Fi 6/6E and UWB channels 5–11 MIMO applications. The proposed MIMO antenna comprises four identical elements arranged in a sequential rotation style. Each element integrates four small patches with two asymmetric notches, enabling the excitation of seven resonant modes to enrich the bandwidth. In addition, we adopt an L-shaped probe feeding method to stimulate these seven modes and employ a circle of blind vias for size miniaturization. Fabricated within compact dimensions of 60.6 × 60.6 × 2 mm$^3$, our MIMO antenna spans the Wi-Fi 6/6E and UWB channels 5–11 bands, ranging from 5.14 to 9.05 GHz, with measured total efficiencies from 43.6% to 85.1%. The isolation between each antenna element surpasses 12 dB, and the ECCs remain below 0.04 within the operating bandwidth. With its attributes including broad bandwidth, compact size, and low profile, the proposed MIMO antenna shows significant potential for supporting multiple wireless services on mobile terminals.

## REFERENCES

[1] W. Zhang, Y. Li, K. Wei, and Z. Zhang, "A two-port microstrip antenna with high isolation for Wi-Fi 6 and Wi-Fi 6E applications," *IEEE Trans. Antennas Propag.*, vol. 70, no. 7, pp. 5227–5234, Jul. 2022.
[2] W. Zhang, Y. Li, K. Wei, and Z. Zhang, "A dual-band MIMO antenna system for 2.4/5 GHz WLAN applications," *IEEE Trans. Antennas Propag.*, vol. 71, no. 7, pp. 5749–5758, Jul. 2023.
[3] W. Zhang, Y. Li, K. Wei, and Z. Zhang, "Dual-band decoupling for two back-to-back PIFAs," *IEEE Trans. Antennas Propag.*, vol. 71, no. 3, pp. 2802–2807, Mar. 2023.

[4] A. Zhang, K. Wei, S. Chu, and Y. Wang, "Extremely compact interconnected half-mode cavity antennas with enhanced isolation for MIMO system," *IEEE Trans. Antennas Propag.*, vol. 70, no. 12, pp. 12264–12269, Dec. 2022.

[5] M. K. Meshram, R. K. Animeh, A. T. Pimpale, and N. K. Nikolova, "A novel quad-band diversity antenna for LTE and Wi-Fi applications with high isolation," *IEEE Trans. Antennas Propag.*, vol. 60, no. 9, pp. 4360–4371, Sep. 2012.

[6] Y. Li, Z. Zhang, J. Zheng, and Z. Feng, "Compact heptaband reconfigurable loop antenna for mobile handset," *IEEE Antennas Wireless Propag. Lett.*, vol. 10, pp. 1162–1165, 2011.

[7] H. S. Singh, M. Agarwal, G. K. Pandey, and M. K. Meshram, "A quad-band compact diversity antenna for GPS L1/Wi-Fi/LTE2500/WiMAX/HIPERLAN1 applications," *IEEE Antennas Wireless Propag. Lett.*, vol. 13, pp. 249–252, 2014.

[8] C. A. Cai, K. Y. Kai, and W. J. Liao, "A WLAN/WiFi-6E MIMO antenna design for handset devices," in *Proc. Int. Symp. Antennas Propag. (ISAP)*, Taipei, Taiwan, 2021, pp. 1–2.

[9] K. Zhao, S. Zhang, K. Ishimiya, Z. Ying, and S. He, "Body-insensitive multimode MIMO terminal antenna of double-ring structure," *IEEE Trans. Antennas Propag.*, vol. 63, no. 5, pp. 1925–1936, May 2015.

[10] A. Zhang, K. Wei, Q. Guan, and Y. Hu, "Compactly placed high-isolated antenna pair with independent control of decoupling amplitude and phase," *IEEE Trans. Antennas Propag.*, vol. 71, no. 3, pp. 2814–2819, Mar. 2023.

[11] D. Q. Liu, M. Zhang, H. J. Luo, H. L. Wen, and J. Wang, "Dual-band platform-free PIFA for 5G MIMO application of mobile devices," *IEEE Trans. Antennas Propag.*, vol. 66, no. 11, pp. 6328–6333, Nov. 2018.

[12] A. Zhang, K. Wei, and Z. Zhang, "Multiband and wideband self-multipath decoupled antenna pairs," *IEEE Trans. Antennas Propag.*, vol. 71, no. 7, pp. 5605–5615, Jul. 2023.

[13] X. Chen, J. Wang, and L. Chang, "Extremely low-profile dual-band microstrip patch antenna using electric coupling for 5G mobile terminal applications," *IEEE Trans. Antennas Propag.*, vol. 71, no. 2, pp. 1895–1900, Feb. 2023.

[14] A. Zhang, K. Wei, Y. Hu, and Q. Guan, "High-isolated coupling-grounded patch antenna pair with shared radiator for the application of 5G mobile terminals," *IEEE Trans. Antennas Propag.*, vol. 70, no. 9, pp. 7896–7904, Sep. 2022.

[15] B. Cheng and Z. Du, "Dual polarization MIMO antenna for 5G mobile phone applications," *IEEE Trans. Antennas Propag.*, vol. 69, no. 7, pp. 4160–4165, Jul. 2021.

[16] B. Cheng and Z. Du, "A wideband low-profile microstrip MIMO antenna for 5G mobile phones," *IEEE Trans. Antennas Propag.*, vol. 70, no. 2, pp. 1476–1481, Feb. 2022.

[17] X. Tian, J. Wang, C. Zheng, and Z. Du, "Shared-radiator wideband grounded patch antenna pair with bending slot for mobile terminals," *IEEE Trans. Antennas Propag.*, vol. 72, no. 4, pp. 3724–3729, Apr. 2024.

[18] I. R. R. Barani, K.-L. Wong, Y.-X. Zhang, and W.-Y. Li, "Low-profile wideband conjoined open-slot antennas fed by grounded coplanar waveguides for 4 × 45 G MIMO operation," *IEEE Trans. Antennas Propag.*, vol. 68, no. 4, pp. 2646–2657, Apr. 2020.

[19] L. Chang and H. Wang, "Miniaturized wideband four-antenna module based on dual-mode PIFA for 5G 4 × 4 MIMO applications," *IEEE Trans. Antennas Propag.*, vol. 69, no. 9, pp. 5297–5304, Sep. 2021.

[20] L. Chang and H. Wang, "Dual-band four-antenna module covering N78/N79 based on PIFA for 5G terminals," *IEEE Antennas Wireless Propag. Lett.*, vol. 21, pp. 168–172, 2022.

[21] C. Deng, "Wideband microstrip antennas loaded by ring resonators," *IEEE Antennas Wireless Propag. Lett.*, vol. 12, pp. 1665–1668, 2013.

[22] M. Chen, L. Chang, and A. Zhang, "Wideband antenna pairs consisting of E-/M-coupling frame monopoles and M-/E-coupling back cover patches for mobile terminal applications," *IEEE Trans. Antennas Propag.*, vol. 72, no. 2, pp. 1308–1318, Feb. 2024.

[23] Y. Chen, S. Yang, and Z. Nie, "Bandwidth enhancement method for low profile E-shaped microstrip patch antennas," *IEEE Trans. Antennas Propag.*, vol. 58, no. 7, pp. 2442–2447, Jul. 2010.

[24] K.-L. Wong and W.-H. Hsu, "A broad-band rectangular patch antenna with a pair of wide slits," *IEEE Trans. Antennas Propag.*, vol. 49, no. 9, pp. 1345–1347, Sep. 2001.

[25] P.-Y. Qin, F. Wei, and Y. J. Guo, "A wideband-to-narrowband tunable antenna using a reconfigurable filter," *IEEE Trans. Antennas Propag.*, vol. 63, no. 5, pp. 2282–2285, May 2015.

[26] Y. Wang et al., "Design of an instantaneous-wideband frequency reconfigurable microstrip antenna based on (Ba, Sr)$TiO_3$/MgO composite thin films," *IEEE Trans. Antennas Propag.*, vol. 62, no. 12, pp. 6472–6475, Dec. 2014.

[27] T. K. Nguyen, C. D. Bui, A. Narbudowicz, and N. Nguyen-Trong, "Frequency-reconfigurable antenna with wide-and narrowband modes for sub-6 GHz cognitive radio," *IEEE Antennas Wireless Propag. Lett.*, vol. 22, pp. 64–68, 2023.

[28] M. Hu and Y. Li, "Wideband back cover microstrip antenna with multiple shorting vias for mobile 5G MIMO applications," *IEEE Trans. Antennas Propag.*, vol. 71, no. 10, pp. 8290–8295, Oct. 2023.

[29] N.-W. Liu, L. Zhu, W.-W. Choi, and X. Zhang, "A low-profile aperture-coupled microstrip antenna with enhanced bandwidth under dual resonance," *IEEE Trans. Antennas Propag.*, vol. 65, no. 3, pp. 1055–1062, Mar. 2017.

[30] Y. Zhang and Y. Li, "Wideband microstrip antenna in small volume without using fundamental mode," *Electromagn. Sci.*, vol. 1, no. 2, pp. 1–6, Jun. 2023.

[31] J. Liu, Q. Xue, H. Wong, H. W. Lai, and Y. Long, "Design and analysis of a low-profile and broadband microstrip monopolar patch antenna," *IEEE Trans. Antennas Propag.*, vol. 61, no. 1, pp. 11–18, Jan. 2013.

[32] Y. Zhang, Y. Li, W. Zhang, Z. Zhang, and Z. Feng, "Omnidirectional antenna diversity system for high-speed onboard communication," *Engineering*, vol. 11, pp. 72–79, Apr. 2022.

[33] W. Liu, Z. N. Chen, and X. Qing, "Metamaterial-based low-profile broadband aperture-coupled grid-slotted patch antenna," *IEEE Trans. Antennas Propag.*, vol. 63, no. 7, pp. 3325–3329, Jul. 2015.

[34] W. E. I. Liu, Z. N. Chen, and X. Qing, "Broadband low-profile L-probe fed metasurface antenna with TM leaky wave and TE surface wave resonances," *IEEE Trans. Antennas Propag.*, vol. 68, no. 3, pp. 1348–1355, Mar. 2020.

[35] W. Sun and Y. Li, "Dual-polarized grid-slotted microstrip antenna with enhanced bandwidth and low profile," *Appl. Comput. Electromagn. Soc. J. (ACES)*, vol. 34, no. 3, pp. 451–456, Mar. 2019.

[36] W. E. I. Liu, Z. N. Chen, and X. Qing, "Broadband circularly polarized metasurface antenna fed by a rotated L-shaped probe," in *Proc. 14th Eur. Conf. Antennas Propag. (EuCAP)*, Copenhagen, Denmark, Mar. 2020, pp. 1–4.

[37] W. Sun, Y. Li, Z. Zhang, and Z. Feng, "Broadband and low-profile microstrip antenna using strip-slot hybrid structure," *IEEE Antennas Wireless Propag. Lett.*, vol. 16, pp. 3118–3121, 2017.

[38] C. L. Mak, K. M. Luk, K. F. Lee, and Y. L. Chow, "Experimental study of a microstrip patch antenna with an L-shaped probe," *IEEE Trans. Antennas Propag.*, vol. 48, no. 5, pp. 777–783, May 2000.

[39] S. Yang, G. Zhang, X. Yue, J. Ru, and G. Fan, "A dual-frequency broadband patch antenna with L-shaped probe feed for 5G communication," in *Proc. Int. Symp. Antennas Propag. (ISAP)*, Xi'an, China, 2019, pp. 1–3.

[40] W. Sun and Y. Li, "Gain stabilization method for wideband slot-coupled microstrip antenna," *IEEE Trans. Antennas Propag.*, vol. 69, no. 12, pp. 8932–8936, Dec. 2021.

[41] Y. Wang and Z. Du, "Dual-polarized slot-coupled microstrip antenna array with stable active element pattern," *IEEE Trans. Antennas Propag.*, vol. 63, no. 9, pp. 4239–4244, Sep. 2015.

[42] J.-H. Park, Y.-H. Ryu, and J.-H. Lee, "Mu-zero resonance antenna," *IEEE Trans. Antennas Propag.*, vol. 58, no. 6, pp. 1865–1875, Jun. 2010.

[43] C.-X. Mao and Q.-X. Chu, "Compact coradiator UWB-MIMO antenna with dual polarization," *IEEE Trans. Antennas Propag.*, vol. 62, no. 9, pp. 4474–4480, Sep. 2014.

[44] L. Liu, S. W. Cheung, and T. I. Yuk, "Compact MIMO antenna for portable UWB applications with band-notched characteristic," *IEEE Trans. Antennas Propag.*, vol. 63, no. 5, pp. 1917–1924, May 2015.

[45] Y.-Y. Liu and Z.-H. Tu, "Compact differential band-notched stepped-slot UWB-MIMO antenna with common-mode suppression," *IEEE Antennas Wireless Propag. Lett.*, vol. 16, pp. 593–596, 2017.

[46] J. Ren, W. Hu, Y. Yin, and R. Fan, "Compact printed MIMO antenna for UWB applications," *IEEE Antennas Wireless Propag. Lett.*, vol. 13, pp. 1517–1520, 2014.

**Kaifeng Li** received the B.S. degree in electronic engineering from Tsinghua University, Beijing, China, in 2024, where he is currently pursuing the Ph.D. degree in electronic engineering.

His current research interests include wideband antennas, microstrip antennas, and metamaterial antennas.

**Yongjian Zhang** received the B.S. degree in communication engineering from Tongji University, Shanghai, China, in 2018, and the Ph.D. degree in electronic engineering from Tsinghua University, Beijing, China, in 2023.

He is currently a Postdoctoral Fellow with the Department of Electronic Engineering, Tsinghua University. His current research interests include aircraft antennas, dual-polarized antennas, and multiple-input and multiple-output (MIMO) antenna arrays.

Dr. Zhang serves as a Reviewer for the IEEE TRANSACTIONS ON ANTENNAS AND PROPAGATION, IEEE ANTENNAS AND WIRELESS PROPAGATION LETTERS, and *Microwave and Optical Technology Letters*.

**Yue Li** (Senior Member, IEEE) received the B.S. degree in telecommunication engineering from Zhejiang University, Zhejiang, China, in 2007, and the Ph.D. degree in electronic engineering from Tsinghua University, Beijing, China, in 2012.

He is currently an Associate Professor with the Department of Electronic Engineering, Tsinghua University. In June 2012, he was a Postdoctoral Fellow with the Department of Electronic Engineering, Tsinghua University. In December 2013, he was a research scholar with the Department of Electrical and Systems Engineering, University of Pennsylvania. He was also a Visiting Scholar with Institute for Infocomm Research (I2R), A*STAR, Singapore, in 2010, and Hawaii Center of Advanced Communication (HCAC), University of Hawaii at Manoa, Honolulu, HI, USA, in 2012. Since January 2016, he has been with Tsinghua University, where he is an Assistant Professor. He has authored and coauthored over 220 journal papers and 50 international conference papers, and holds 26 granted Chinese patents. His current research interests include metamaterials, plasmonics, electromagnetics, nanocircuits, mobile and handset antennas, MIMO and diversity antennas, and millimeter-wave antennas and arrays.

Dr. Li was a recipient of the Issac Koga Gold Medal from URSI General Assembly in 2017; the Young Scientist Award from the conferences of Progress in Electromagnetics Research Symposium (PIERS) 2019, International Applied Computational Electromagnetics Society Symposium (ACES) 2018, Atlantic Radio Science Conference (AT-RASC) 2018, Asia-Pacific Radio Science Conference (AP-RASC) 2016, International Symposium on Electromagnetic Theory (EMTS) 2016, and URSI General Assembly and Scientific Symposium (GASS) 2014. He served as an Associate Editor for the IEEE TRANSACTIONS ON ANTENNAS AND PROPAGATION, IEEE ANTENNAS AND WIRELESS PROPAGATION LETTERS from 2017 to 2024. He is serving as an Associate Editor for *Microwave and Optical Technology Letters*, and *Computer Applications in Engineering Education*.